International Journal of Solids and Structures xxx (xxxx) xxx

Contents lists available at ScienceDirect

International Journal of Solids and Structures

journal homepage: www.elsevier.com/locate/ijsolstr

A variational phase-field model for brittle fracture in polydisperse elastomer networks

Bin Li, Nikolaos Bouklas*

Sibley School of Mechanical and Aerospace Engineering, Cornell University, NY 14853, USA

ARTICLE INFO

Article history:
Received 17 March 2019
Revised 23 June 2019
Accepted 12 August 2019

Keywords:
Chain length distribution
Equal force
Elastomer networks
Phase-field model
Brittle fracture
Incompressible

ABSTRACT

The distribution of chain lengths in elastomer networks occurs naturally during polymerization, and has a critical role in the mechanical behavior of these materials, including the damage and fracture response. A common underlying assumption for the majority of constitutive models for rubber elasticity is that all the chains admit the same length. Moreover, in the classical statistical mechanical model for elastomer networks, the changes in internal energy are generally assumed to be negligible in comparison to the changes in configurational entropy. In contrast, the fracture process in a elastomer network, as already demonstrated in the well-known Lake-Thomas model, is essentially internal energy dominated. In this paper, we formulate a phase-field model for brittle fracture in polydisperse elastomer networks extending and merging recent advances in the fields of (a) homogenization of elastomer networks and (b) the variational approach to brittle fracture, allowing for predictions of crack nucleation, initiation and propagation. The free energy of the continuum is obtained employing an eight chain network model, accounting for (a) internal energy contributions from the extension of molecular bonds and (b) arbitrary chain length distribution. The representative chain in the eight chain network model takes into account the distribution of chain lengths, following the recently developed equal force model. We employ a mixed displacement-pressure formulation for the discretization of the incompressible large deformation elastic problem that arises. The analytical solution for the crack nucleation problem of an incompressible hyperelastic bar under uniaxial loading is compared with the three-dimensional simulation result. Finally, we demonstrate through a representative numerical simulation the capability of the gradient damage model to simulate crack propagation in an incompressible elastomer network.

1. Introduction

In addition to traditional engineering applications, elastomers and hydrogels where the polymer network provides a permanent three-dimensional structure, have been widely used in biomedical applications such as hydrogel scaffolds for tissue engineering (Drury and Mooney, 2003), artificial soft tissues (e.g. articular cartilage and ligaments) (Lynch et al., 2017) and as implants for damaged soft-tissue repair (Nonoyama et al., 2016) where they serve a load-bearing function. All these applications demand a better understanding of the mechanical properties and development of physically motivated mathematical models for predicting damage and failure of these materials. Therefore, an accurate constitutive model is essential for studying the mechanical response of elastomer networks. A common underlying assumption for the majority of constitutive models for rubber elasticity (James and Guth, 1943; Wu and Van Der Giessen, 1993; Boyce and Arruda, 2000) is that all the chains admit the same length, i.e. the same number of Kuhn segments. However, all synthetic polymers are polydisperse in that they contain polymer chains of unequal length, characterized by a chain-length distribution functions (Flory, 1953; Watson, 1953; Falender et al., 1979). The chain length distribution originates from the randomness of the polymerization process.

Experiments and theoretical works have shown that the mechanical (Falender et al., 1979; Mark, 2003; Higgs and Ball, 1988; Tehrani and Sarvestani, 2017), damage and fracture behaviors (Mark, 2003; Itskov and Knyazeva, 2016; Tehrani and Sarvestani, 2017), as well as mechanochemical properties (Wang et al., 2015) of elastomer networks depend on the distribution of the chain lengths between crosslinks. For this reason, it is crucial for constitutive models to take into account the chain lengths distribution. Some constitutive models based upon statistical mechanics considerations (James and Guth, 1943; Treloar, 1975) have been developed, in which the idealized networks are assembled following an

* Corresponding author.
E-mail address: nb589@cornell.edu (N. Bouklas).

https://doi.org/10.1016/j.ijsolstr.2019.08.012
0020-7683/

equal strain assumption, which corresponds to a parallel arrangement of chains of different lengths, where all chains assume the same stretch (Zhao, 2012; Wang et al., 2015; Itskov and Knyazeva, 2016; Tehrani and Sarvestani, 2017). However, such schemes result in large values of force and even diverged values of force for chains that their prescribed end-to-end length is beyond their contour length (Verron and Gros, 2017). One can remedy this issue by restricting the end-to-end length to be less than the contour length of short chains (Diani and Le Tallec, 2019), or by accounting for chain rupture at some finite stretch (Zhao, 2012; Itskov and Knyazeva, 2016; Tehrani and Sarvestani, 2017). Other works propose the equal force assumption (von Lockette et al., 2002), corresponding to a series arrangement of "sub-chains" of varying chain length into a "master" chain where the sub-chains carry the same force. Adopting the equal force assumption, Verron and Gros (2017) derived an affine full-network model of non-Gaussian randomly jointed chains with arbitrary chain length distribution.

Although elastomer networks are capable of sustaining large deformations, they are often found to fracture in a brittle manner, which greatly limits their application potential in the biomedical field. In line with the Griffith theory of brittle fracture, Rivlin and Thomas (1953) experimentally quantified the macroscopic fracture toughness or tearing energy of rubber. The macroscopic fracture toughness of crosslinked elastomers was calculated by Lake and Thomas (1967) based on the assumption that the polymer chains lying across the plane of crack propagation at the front of a crack are stretched, and all the chemical bonds along the chains are pulled to a certain critical extension prior to chains rupture. The experimental measurements carried out under near equilibrium conditions (Mueller and Knauss, 1971; Ahagon and Gent, 1975) have found reasonably good agreement with the simple model of Lake and Thomas (1967). The success of the model of Lake and Thomas (1967) suggests that the fracture process of elastomer networks is internal energy dominated. However, the classical statistical mechanical model for the elasticity of elastomer networks consider only the change in the configurational entropy and generally assume that internal energy changes are negligible compared to entropy changes; the two assumptions cannot be directly reconciled without further considerations. To address this problem, Mao et al. (2017) developed a rational yet simple model that describes the entropic elasticity of elastomer networks and recovers the Lake and Thomas (1967) scaling law for the macroscopic fracture toughness in the presence of a macroscopic crack.

The prediction of crack initiation and propagation in elastomer networks is of great importance for engineering applications. Computational approaches to brittle fracture mechanics require criteria to predict the onset of crack initiation, the direction of crack propagation and possibly crack branching under dynamic loading conditions. Moreover, specialized techniques are necessary to numerically represent and track sharp cracks, such as sophisticated adaptive remeshing schemes that introduce new boundaries when the crack propagates (Ingraffea and Saouma, 1985; Chen et al., 2018; 2019) or local enrichment of the approximation space to account for discontinuities and asymptotic fields in the extended finite element method (Moës et al., 1999). In recent years, gradient damage or phase-field models of fracture (Bourdin et al., 2000; Marigo et al., 2016), founded on the variational approach to brittle fracture proposed by Francfort and Marigo (1998), have emerged as a promising approach to computational fracture mechanics. In these models, the complexity of tracking and evolving cracks is addressed by introducing an additional field variable describing cracks in a smeared way, which leads to an additional partial differential equation coupled to the equilibrium equation of elasticity.

In this paper we develop a micromechanically motivated phase-field model for fracture in polydisperse elastomers. We start from an extensible randomly jointed chain model recently proposed by Smith et al. (1996) and extended to polymers to allow for stretch of Kuhn segments by Mao et al. (2017) and modify it by formulating a hybrid extensible randomly jointed chain model taking into account the distribution of chain lengths. This hybrid single chain model corresponds to a series arrangement of chains such that the chains of different length carry the same force between crosslinks (Verron and Gros, 2017). Following, we extend it to a continuum model through the use of eight chain network averaging (Arruda and Boyce, 1993) and discuss the effects of chain length distribution on the mechanical properties and fracture toughness in Section 2. We couple the derived free energy to a phase-field model formulated on the undeformed or reference configuration in Section 3. Section 4 succinctly describes the numerical implementation of the model. We provide[1] an open-source numerical implementation of the proposed phase-field model based on `FEniCS` platform (Alnæs et al., 2015), where the numerical difficulties associated to the volumetric locking in incompressible materials are solved by using a mixed displacement-pressure formulation. Section 5 presents representative simulations, demonstrating the capability of the developed phase-field model for fracture in polydisperse elastomer networks in problems including crack nucleation, initiation and propagation.

2. Elastic deformation and fracture toughness

The statistical mechanics approach to derive a constitutive model for elastomer networks starts from the study of the statistical properties of a randomly jointed long-chain molecule (Treloar, 1975). The non-Gaussian treatment of a single long-chain (James and Guth, 1943; Treloar, 1975), which circumvents the inherent limitations of the Gaussian chain model, accounts for the finite extensibility of the chain at deformations where the end to end length $\|\boldsymbol{r}\|$ begins to approach the fully extended length Nb. The Helmholtz free energy (James and Guth, 1943; Flory, 1953; Treloar, 1975) of a single chain having randomly jointed N number of Kuhn segments of equal length b is determined by

$$\psi(\boldsymbol{r}) = kTN\left(\frac{\|\boldsymbol{r}\|}{Nb}\beta + \ln\frac{\beta}{\sinh\beta}\right), \quad \beta = \mathscr{L}^{-1}\left(\frac{\|\boldsymbol{r}\|}{Nb}\right), \tag{1}$$

where T is the absolute temperature, k is the Boltzmann constant, an arbitrary constant is omitted as being unimportant, and $\mathscr{L}$ denotes the Langevin function defined as $\mathscr{L}(x) = \coth(x) - 1/x$. Thus the non-Gaussian tensile force acting along the direction of vector $\boldsymbol{r}$ follows as

$$f = \frac{kT}{b}\mathscr{L}^{-1}\left(\frac{\|\boldsymbol{r}\|}{Nb}\right). \tag{2}$$

The physically motivated polymer network models built on the microscopic response of individual long-chain molecules (Treloar and Riding, 1979; Arruda and Boyce, 1993; Wu and Van Der Giessen, 1993; Boyce and Arruda, 2000) showed a pronounced ability to capture the response of experimental data in three distinct deformation modes, namely uniaxial, equibiaxial and pure shear, at large strains. Note that in the aforementioned models as the chain length approaches the contour length, or in other words tends to completely straight configuration, $\|\boldsymbol{r}\| \to Nb$, the free energy (1) as well as the chain force (2) diverge. Therefore, the application of the non-Gaussian chain model is restricted by the condition, $\|\boldsymbol{r}\| < Nb$. The free energy functional (1), without doubt, does not allow for the breaking of chemical bonds in the chain backbone, which in general occurs at larger chain stretch such that the chain is extended beyond its contour length (Crist et al., 1984; Mao et al., 2017), restricting the direct application of such models towards damage and fracture modeling.

[1] https://bitbucket.org/bin-mech/gradient_damage_polymer/.

Please cite this article as: B. Li and N. Bouklas, A variational phase-field model for brittle fracture in polydisperse elastomer networks, International Journal of Solids and Structures, https://doi.org/10.1016/j.ijsolstr.2019.08.012

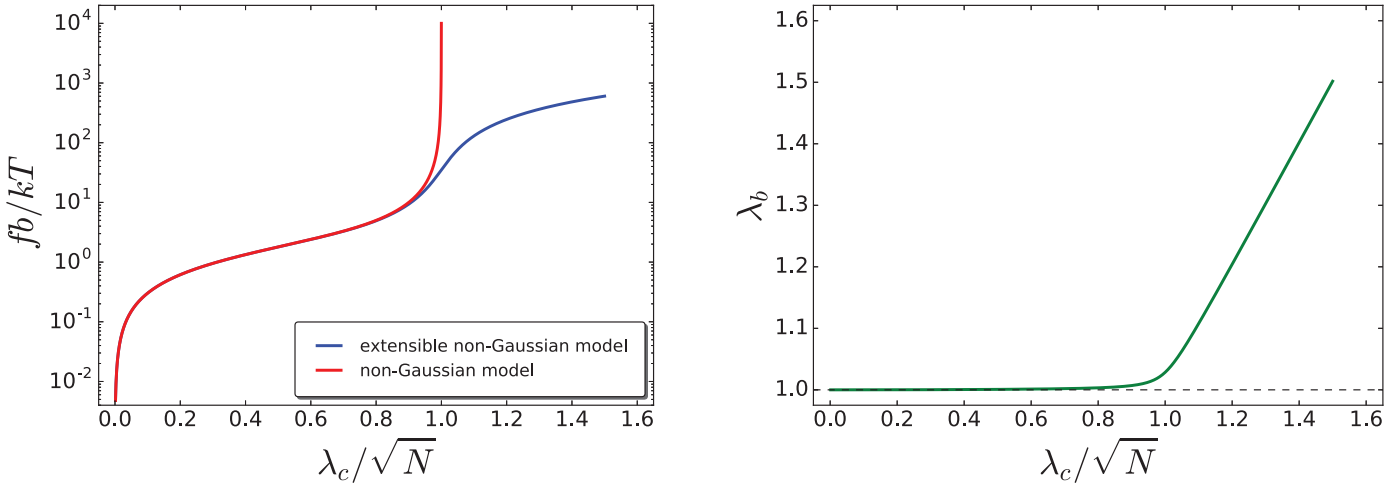

Fig. 1. The normalized chain force fb/kT, scaled logarithmically, versus normalized chain stretch $\lambda_c/\sqrt{N}$ (left). The Kuhn segments stretch λ_b versus normalized chain stretch $\lambda_c/\sqrt{N}$ (right).

2.1. Free energy of an extensible randomly jointed chain

To model the rupture of elastomer networks by scission of bonds in the chain backbone, Mao et al. (2017) adapted the idea of Smith et al. (1996) which was applied to the modeling of "over-stretching" of DNA molecules to relax the rigidity assumption of the individual Kuhn segment. They modified the randomly jointed chain model by taking into account the deformation of the Kuhn segments as well as the effect of alignment under tensile loading. Specifically, the free energy of a single chain accounting for the elongation of Kuhn segments takes the form (Mao et al., 2017)

$$\psi(\boldsymbol{r},\lambda_b) = U(\lambda_b) + kTN\left(\frac{\|\boldsymbol{r}\|}{N\lambda_b b}\beta + \ln\frac{\beta}{\sinh\beta}\right),$$
$$\beta = \mathscr{L}^{-1}\left(\frac{\|\boldsymbol{r}\|}{N\lambda_b b}\right), \tag{3}$$

where λ_b is a dimensionless stretch ratio of the Kuhn segments. Introducing the notation of the overall chain stretch $\lambda_c = \|\boldsymbol{r}\|/\|\boldsymbol{r}_0\|$ and the unstretched chain length $\|\boldsymbol{r}_0\| = \sqrt{N}b$ given by the square root of the mean-square value of end-to-end distance (Treloar, 1975). The free energy functional (3) can be rewritten in terms of the overall chain stretch λ_c as

$$\psi(\lambda_c,\lambda_b) = U(\lambda_b) + kTN\left(\frac{\lambda_c\lambda_b^{-1}}{\sqrt{N}}\beta + \ln\frac{\beta}{\sinh\beta}\right),$$
$$\beta = \mathscr{L}^{-1}\left(\frac{\lambda_c\lambda_b^{-1}}{\sqrt{N}}\right). \tag{4}$$

In comparison of the extensible free energy functional (4) and the classical energy functional (1), the modified stretch $\lambda_c\lambda_b^{-1}$ can be interpreted as the chain stretch due solely to the rearrangement of Kuhn segments (Mao et al., 2017; Talamini et al., 2018), neglecting the internal energy of bond stretching. In the following, we will assume that the internal energy of the chain is modeled employing a simple functional form as in Talamini et al. (2018) and Mao and Anand (2018)

$$U(\lambda_b) = \frac{1}{2}NE_b(\lambda_b - 1)^2, \tag{5}$$

although different choices are possible, see e.g. Mao et al. (2017) and Dal and Kaliske (2009). The constant E_b denotes the stiffness of the chemical bonds in the chain backbone and has units of energy.

Under given overall chain stretch $\lambda_c = \bar{\lambda}_c$, the stretch λ_b of the Kuhn segments is dictated by the competition between the internal energy contribution and the entropic contribution to the free energy (4). Accordingly, given the overall chain stretch λ_c, the segment stretch λ_b is sought as the minimizer of the energy functional (4), i.e. $\lambda_b = \arg\min_{\lambda_b\geq 1}\tilde{\psi}(\lambda_b)$, being $\tilde{\psi}(\lambda_b) := \{\psi(\lambda_c,\lambda_b),\ \lambda_c = \bar{\lambda}_c\}$. The expression for the chain force in terms of the chain stretch λ_c is given by

$$f = \frac{kT}{\lambda_b b}\mathscr{L}^{-1}\left(\frac{\lambda_c\lambda_b^{-1}}{\sqrt{N}}\right). \tag{6}$$

Fig. 1 shows the comparison of the force response of the extensible randomly jointed chain model with the classical non-Gaussian chain model (with $E_b/kT = 1200$). As is shown from Fig. 1(left), the extensible chain model distinguishes from the classical model at stretches $\lambda_c \geq 0.9\sqrt{N}$, nevertheless, the Kuhn segment stretch λ_b becomes significant as $\lambda_c \to \sqrt{N}$, see the Fig. 1(right), which regularizes the divergent behavior of the classic model. For a detailed discussion on the extensible chain model, we refer the interested reader to Mao et al. (2017).

2.2. Free energy of polydisperse elastomer networks

Most polymers are polydisperse in that they consist of polymer chains of unequal length (different number of Kuhn segments), usually characterized by a chain length distribution (Flory, 1953; Watson, 1953; Falender et al., 1979). A common underlying assumption for a great majority of constitutive models for elastomer networks is that all the chains admit the unique same length. These idealized models are unable to accurately capture the mechanical response of polydisperse elastomer networks (von Lockette et al., 2002; Verron and Gros, 2017). Some constitutive models have been developed, in which the idealized networks of different chain lengths are assembled following an equal length assumption corresponding to a parallel arrangement of chains with different lengths (see e.g. Zhao, 2012; Wang et al., 2015; Itskov and Knyazeva, 2016; Tehrani and Sarvestani, 2017). This assumption practically is well-adapted to the derivation of constitutive equations, the free energy and the stress are merely the summation of the contributions of the different networks. However, such schemes result in diverging chain force values for short chains, as their prescribed end-to-end length grow beyond their contour length for large macroscopic stretch values (Verron and Gros, 2017).

Please cite this article as: B. Li and N. Bouklas, A variational phase-field model for brittle fracture in polydisperse elastomer networks, International Journal of Solids and Structures, https://doi.org/10.1016/j.ijsolstr.2019.08.012

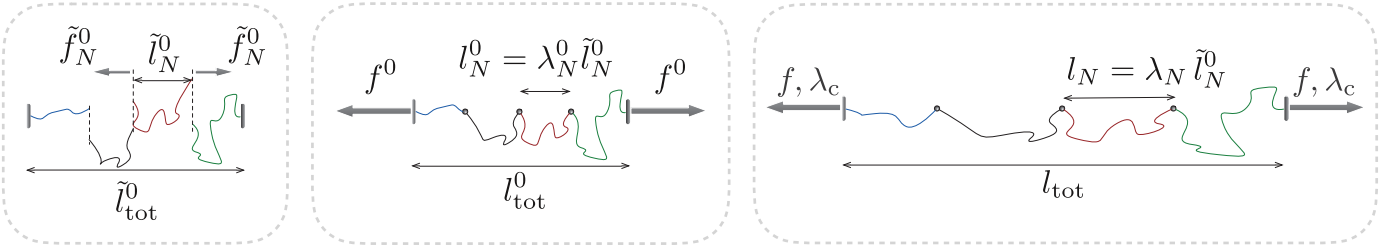

Fig. 2. Schematic diagram of three successive states of a representative chain. (left) The chains are at equilibrium prior to assembly. (center) the chains are assembled and respect the equal force assumption in the unstrained/reference conformation. (right) the representative chain is stretched allowing for the possibly of a non-zero Kuhn segment stretch. Source: Adapted from Verron and Gros (2017).

Given the aforementioned limitations of the equal length assumption, here we adopt the equal force assumption (Verron and Gros, 2017), corresponding to a series arrangement of polymer chains. We consider a polymer network comprised of idealized sub-networks; where each sub-network only contains chains with exactly N Kuhn segments. For convenience we introduce $P(N)$, the chain length distribution which is given as the number fraction of chains with N monomers with respect to the total number of polymer chains so that $\sum_{N=N_0}^{\infty} P(N) = 1$, $n(N)$, the number density of the sub-network of chains with N Kuhn segments, $V(N)$, the volume fraction of the sub-network of chains with N Kuhn segments such that $\sum_{N=N_0}^{\infty} V(N) = 1$, as well as the total chain density $n = \sum_{N=N_0}^{\infty} n(N)V(N)$.

The representative hybrid chain used to realize the equal force assumption is defined as the connection of chains as illustrated in Fig. 2, where the chain length distribution of the constituent chains follows that of the whole network. Moreover, the equal fore assumption necessitates that the deformed/current end-to-end vector of any sub-chain is collinear with the deformed end-to-end vector of the representative chain, illustrated in Fig. 2(right).

In order to derive the chain force versus stretch equation for the representative chain, as in Verron and Gros (2017), three successive states are considered as shown in Fig. 2 and described as follows.

(1) The sub-chains (referring to individual chains that will be combined to form the representative hybrid chain) are all in their unstrained configuration and they are not assembled, see Fig. 2(left). Thus we have the individual chain length at this stage given by $\tilde{l}^0_N = \sqrt{N}b$, and plugging into (2) gives the entropic force on each of the sub-chains as $\tilde{f}^0_N = kT/b\,\mathscr{L}^{-1}\left(1/\sqrt{N}\right)$. The stretch of the sub-chains at this state is $\tilde{\lambda}^0_N = 1$. Because of the entropic nature of the randomly jointed chain model, a non-vanishing force is required to keep the end-to-end distance unchanged, consequently, chain force $\tilde{f}^0_N$ varies with respect to N. Assuming that the sub-chains have aligned end-to-end vectors, the total length of the representative hybrid chain at this state can be calculated as $\tilde{l}^0_{\rm tot} = \sum_{N=N_0}^{\infty} P(N)\tilde{l}^0_N = \sum_{N=N_0}^{\infty} P(N)\tilde{\lambda}^0_N\sqrt{N}b = \sum_{N=N_0}^{\infty} P(N)\sqrt{N}b$; this is a necessary assumption for the following steps.

(2) The sub-chains are assembled into a representative hybrid chain and respect the equal force assumption, see Fig. 2(center) and the hybrid chain is considered to be in its reference state. At this state we postulate that the bond stretch $\lambda^N_b = 1$ in sub-chains with N Kuhn segments as none of the sub-chains are approaching their locking stretch, as deviation from $\lambda^N_b = 1$ is only expected when chains are approaching their locking stretch. The attentive reader will have suspected that even in the reference state the Kuhn segments are also possibly stretched; we will rationalize the postulation in Remark 1. Assuming that a non-zero force f^0 is exerted on the assembly we have $f^0_N = f^0$ for each sub-chain of N Kuhn segments. The stretch ratio of each sub-chain follows $\lambda^0_N = \sqrt{N}\,\mathscr{L}\left(f^0 b/kT\right)$. The total length of the assembled representative hybrid chain is calculated as $l^0_{\rm tot} = \sum_{N=N_0}^{\infty} P(N) l^0_N = \sum_{N=N_0}^{\infty} P(N)\lambda^0_N\sqrt{N}b = \sum_{N=N_0}^{\infty} P(N)Nb\,\mathscr{L}\left(f^0 b/kT\right)$.

To connect the reference state of a representative hybrid chain to the reference state of the individual sub-chains we consider that $\tilde{l}^0_{\rm tot} = l^0_{\rm tot}$, and introducing the following notation $\sqrt{\mathscr{N}} = \sum_{N=N_0}^{\infty} P(N)N/\sum_{N=N_0}^{\infty} P(N)\sqrt{N}$, we arrive to $\lambda^0_N = \sqrt{N/\mathscr{N}}$. As already pointed out by Verron and Gros (2017), the stretch λ^0_N demonstrates that in the reference state (corresponding to the second stage described in this section), short chains ($N < \mathscr{N}$) are under compression, i.e. $\lambda^0_N < 1$, while the long chains ($N > \mathscr{N}$) are under tension, i.e. $\lambda^0_N > 1$. This clearly emphasizes the hierarchical/nonaffine nature of the representative chain.

Remark 1. In the reference state (2), only the long chains ($N > \mathscr{N}$) are under stretched. Among the stretched long chains, the Kuhn segments are stretched only in the vicinity of $\lambda^0_N \nearrow \sqrt{N}$, i.e. in the setting of $\sqrt{\mathscr{N}} \to 1$. As shown latter $\sqrt{\mathscr{N}} \geq \sum_{N=N_0}^{\infty} P(N)\sqrt{N}$, and in the real polydisperse elastomer networks $\sqrt{\mathscr{N}} \gg 1$, thus the Kuhn segments are not stretched.

(3) The representative hybrid chain is stretched beyond the reference configuration. The chain force is designated by f and the length of sub-chains with N Kuhn segments by l_N. The stretch ratio of the representative chain is written as $\lambda_c = l_{\rm tot}/l^0_{\rm tot}$ and is computed with respect to the unstrained chain length defined in (2). Note that in the current state, the Kuhn segments are also possibly deformed, therefore, the chain force is determined by (6) and respects the equal force assumption

$$f_N = \frac{kT}{\lambda^N_{\rm b} b}\,\mathscr{L}^{-1}\left(\frac{\lambda_N}{\lambda^N_{\rm b}\sqrt{N}}\right) = f. \tag{7}$$

Recalling that segment stretch is determined by $\lambda^N_{\rm b} = \arg\min_{\lambda^N_{\rm b}\geq 1} \tilde{\psi}(\lambda^N_{\rm b})$, the first-order optimal condition leading to

$$E_{\rm b}\left(\lambda^N_{\rm b} - 1\right)\lambda^N_{\rm b} = \frac{kT}{\lambda^N_{\rm b}}\frac{\lambda_N}{\sqrt{N}}\,\mathscr{L}^{-1}\left(\frac{\lambda_N}{\lambda^N_{\rm b}\sqrt{N}}\right), \tag{8}$$

thus the force stretch relation (7) may be reformulated as

$$f_N = \frac{E_{\rm b}}{b}\frac{\sqrt{N}}{\lambda_N}\left(\lambda^N_{\rm b} - 1\right)\lambda^N_{\rm b} = f. \tag{9}$$

Which immediately implies that $\lambda_N/\sqrt{N} = \xi\left(\lambda^N_{\rm b} - 1\right)\lambda^N_{\rm b}$, with a proportionality constant ξ. Using this back in (8), we obtain

$$\lambda^N_{\rm b} = \frac{kT\xi}{E_{\rm b}}\,\mathscr{L}^{-1}\left(\xi\left(\lambda^N_{\rm b} - 1\right)\right). \tag{10}$$

The fact that the solution to (10) does not depend on N, necessitates that the ratio $\lambda_N/\sqrt{N}$ and the segment stretch $\lambda^N_{\rm b}$ are invariant with respect to the number N of Kuhn segments in each sub-chain. Thus in the following we omit the superscript N and

Please cite this article as: B. Li and N. Bouklas, A variational phase-field model for brittle fracture in polydisperse elastomer networks, International Journal of Solids and Structures, https://doi.org/10.1016/j.ijsolstr.2019.08.012

write

$$f_N = \frac{kT}{\lambda_b b}\mathscr{L}^{-1}\left(\frac{\lambda_N\lambda_b^{-1}}{\sqrt{N}}\right) = f. \tag{11}$$

Note that the above arguments do not depend on the specific functional form of the internal energy.

By inverting the chain force equation, the stretched chain length reads

$$l_{\text{tot}} = \sum_{N=N_0}^{\infty} P(N) l_N = \sum_{N=N_0}^{\infty} P(N)\lambda_N\sqrt{N}b = \sum_{N=N_0}^{\infty} P(N)N\lambda_b b\,\mathscr{L}\left(\frac{f\lambda_b b}{kT}\right). \tag{12}$$

Invoking that $l_{\text{tot}}^0 = \tilde{l}_{\text{tot}}^0 = \sum_{N=N_0}^{\infty} P(N)\sqrt{N}b$, the chain force versus stretch of the representative chain is

$$f = \frac{kT}{\lambda_b b}\mathscr{L}^{-1}\left(\frac{\lambda_c\lambda_b^{-1}}{\sqrt{\mathscr{N}}}\right). \tag{13}$$

By comparing (11) and (13) of the chain force, we find that

$$\frac{\lambda_N}{\sqrt{N}} = \frac{\lambda_c}{\sqrt{\mathscr{N}}}, \tag{14}$$

which is a kinematic constraint for the deformation of the sub-chains and crucial for explicitly writing out the free energy of a representative chain.

The Helmholtz free energy of a representative hybrid chain $\psi(\lambda_c, \lambda_b)$ is given by summation of the free energy contributions of the sub-chains (von Lockette et al., 2002), i.e. $\psi(\lambda_c, \lambda_b) = \sum_{N=N_0}^{\infty} P(N)\psi(\lambda_N, \lambda_b)$. Recalling that the free energy of an extensible chain is given by relations (4) and (14), we have

$$\psi(\lambda_c, \lambda_b) = \frac{1}{2}\mathscr{C}\mathscr{N}E_b(\lambda_b - 1)^2 + \mathscr{C}k\mathscr{N}T\left(\frac{\lambda_c\lambda_b^{-1}}{\sqrt{\mathscr{N}}}\beta + \ln\frac{\beta}{\sinh\beta}\right),$$
$$\beta = \mathscr{L}^{-1}\left(\frac{\lambda_c\lambda_b^{-1}}{\sqrt{\mathscr{N}}}\right), \tag{15}$$

where we introduced the following notation $\mathscr{C} = \left(\sum_{N=N_0}^{\infty} P(N)\sqrt{N}\right)^2 / \sum_{N=N_0}^{\infty} P(N)N$. We note that, by comparing free energy (4) of an standard extensible chain and (15) of an extensible hybrid chain, the hybrid chain admits a different stiffness than the standard extensible chain of $\mathscr{N}$ Kuhn segments of bond length $\mathscr{C}b$ (Verron and Gros, 2017). Furthermore, note that $\text{Var}\left(\sqrt{N}\right) = \sum_{N=N_0}^{\infty} P(N)N - \left(\sum_{N=N_0}^{\infty} P(N)\sqrt{N}\right)^2 \geq 0$, thus the parameter $\mathscr{C} \leq 1$ (that was not explicitly stated in Verron and Gros (2017)), has softening effect; the equality holds when the variance of $\sqrt{N}$ vanishes.

To incorporate the representative chain statistics into a constitutive framework, we proceed to employ the eight-chain network model developed by Arruda and Boyce (1993) that represents a polymer network as a collection of identical unit cells. In the undeformed state, the unit cell has eight polymer chains radiating outward from the center to the vertices of the unit cube. Assume that the edges of the cube are parallel to the principal axes of stretch. The assumption of affine deformations leads to the following relation $\lambda_c = \sqrt{\left(\lambda_1^2 + \lambda_2^2 + \lambda_3^2\right)/3} = \sqrt{\text{tr}(\boldsymbol{F}\boldsymbol{F}^T)/3}$, where λ_1, λ_2, λ_3 are the principal stretches of the macroscopic deformation gradient tensor $\boldsymbol{F}$. The Helmholtz free energy of the polydisperse elastomer networks per unit reference volume is

$$W(\boldsymbol{u}, \lambda_b) = \frac{1}{2}\mathscr{C}\mathscr{N}E(\lambda_b - 1)^2 + \mathscr{C}\mathscr{N}\mu\left(\frac{\lambda_c\lambda_b^{-1}}{\sqrt{\mathscr{N}}}\beta + \ln\frac{\beta}{\sinh\beta}\right),$$
$$\beta = \mathscr{L}^{-1}\left(\frac{\lambda_c\lambda_b^{-1}}{\sqrt{\mathscr{N}}}\right), \tag{16}$$

where $\mu = nkT$ denotes the shear modulus and $E = nE_b$ is the bond stretch stiffness of the polymer network. The segment stretch λ_b is determined by setting $\partial W(\lambda_b, \boldsymbol{u})/\partial\lambda_b = 0$, resulting in an implicit nonlinear algebraic equation for λ_b, which reads

$$E(\lambda_b - 1)\lambda_b = \mu\frac{\lambda_c\lambda_b^{-1}}{\sqrt{\mathscr{N}}}\mathscr{L}^{-1}\left(\frac{\lambda_c\lambda_b^{-1}}{\sqrt{\mathscr{N}}}\right). \tag{17}$$

For monodisperse elastomer networks, namely with only one chain length equal to $\mathscr{N}$ corresponding to Dirac delta distribution $P(N) = \delta(N - \mathscr{N})$, the free energy reduces to the one employed in Talamini et al. (2018).

2.3. Fracture toughness of polydisperse elastomer networks

Rivlin and Thomas (1953), applying the Griffith energy balance criterion to rubber materials, experimentally quantified the macroscopic fracture toughness / tearing energy of rubber. In a pioneering contribution, Lake and Thomas (1967) shown that this macroscopic fracture toughness could be calculated approximately by considering the energy required to rupture the polymer chains lying across the path of the crack. They posited that in order to break a particular bond within a polymer chain it is necessary to subject all other bonds lying in the same chain to the rupture force. If the energy required to break a segment is Ξ, then to rupture a chain containing N segments will be approximately $N\Xi$ (Lake and Thomas, 1967), even though only one of these segments will break eventually, as discussed in the analysis of Crist et al. (1984). If the number of chains crossing the unit area in the unstrained state is N_Γ, and assuming that all chains have the same number of Kuhn segments N then the required fracture energy is written as (Lake and Thomas, 1967)

$$G_c := N_\Gamma N\Xi. \tag{18}$$

It is noteworthy that G_c gives the *lower bound* of the energy required to cause unit new surface area in the unstrained state, neglecting plastic and viscous effects in the vicinity of the crack tip. As a first approximation the energy released in the chains which are in the neighborhood of the ruptured chains, are also neglected. The experimental measurements carried out under near equilibrium conditions (Mueller and Knauss, 1971; Ahagon and Gent, 1975) have found reasonably good agreement with the approximation (18).

The number N_Γ of chains crossing per unit area is estimated as follows. In the reference state, the chains are randomly oriented, and the probability of a chain having the end-to-end vector $\boldsymbol{r}$ is characterized by a Gaussian distribution (Treloar, 1975). The mean end-to-end distance of a chain (Lake and Thomas, 1967) is $\|\bar{\boldsymbol{r}}\| = \sqrt{8N/3\pi}b$. For a fixed angle θ, the chain will intersect with the plane of crack propagation if the distance d from the center O to the crack propagation plane belongs to $[0, \|\bar{\boldsymbol{r}}\|/2\sin\theta)$, see Fig. 3. Assume a perfectly uniform network such that all chains have the same mean end-to-end distance $\|\bar{\boldsymbol{r}}\|$ and contain the same number of segments N. Thus the probability of a chain crossing the crack plane is calculated by $\int_0^{\pi/2}\|\bar{\boldsymbol{r}}\|/2\sin\theta\,d\theta = \|\bar{\boldsymbol{r}}\|/2$. Consequently, the number of chains crossing the unit crack surface area is $N_\Gamma = n\sqrt{2N/3\pi}b$ and thus the fracture energy (18) becomes

$$G_c := n\sqrt{\frac{2N}{3\pi}}bN\Xi. \tag{19}$$

This scaling law has been reproduced by Mao et al. (2017), where the authors also resorted to the extensible randomly jointed chain model, and is consistent with the microscopic bond rupture criterion. For polydisperse elastomer networks, all the bonds are stretched up to the rupture force in order for a macroscopic crack to form, which implies that all the chains are stretched to the same

Please cite this article as: B. Li and N. Bouklas, A variational phase-field model for brittle fracture in polydisperse elastomer networks, International Journal of Solids and Structures, https://doi.org/10.1016/j.ijsolstr.2019.08.012

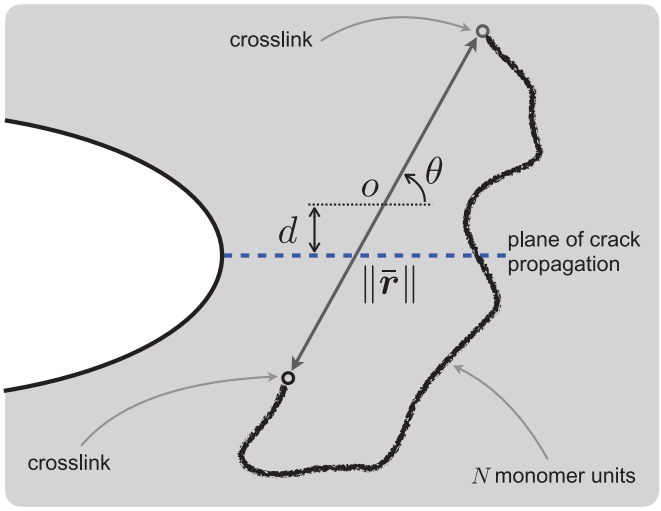

Fig. 3. Schematic diagram of a polymer chain intersecting the plane of crack propagation, where O is the center of the end-to-end distance of the chain.

force. Accordingly the fracture energy takes the form

$$G_c := \sum_{N=N_0}^{\infty} n(N)V(N)N_\Gamma N\Xi = \sum_{N=N_0}^{\infty} nP(N)\sqrt{\frac{2N}{3\pi}}bN\Xi. \tag{20}$$

Remark 2. As stated in Lake and Thomas (1967), in order to break a particular bond within the chain, it is necessary to subject all other bonds lying in the same chain to the rupture force. This assumption is in-line with the equal force condition for the chains in polydisperse elastomer networks, and the fact that the bond stretch of sub-chains is invariant to sub-chain length. Thus the proposed equal force model is intrinsically compatible with the argument that was proposed in the seminal work of Lake and Thomas (1967) to arrive at the surface energy (19) of monodisperse elastomer networks.

From (16) and (17) it is evident that the stress-strain response depends on the chain length distribution $P(N)$ in terms of parameters $\mathscr{C}$ and $\mathscr{N}$, and the total chain density n. The effective shear modulus of the polydisperse elastomer networks is defined as $\mu^* = \mathscr{C}\mu = \mathscr{C}nkT$, and fracture toughness $G_c{}^*$ is given by (20). In Table 1 a set of corresponding chain length distributions, i.e. exponential, uniform, Weibull, normal and log-normal, shown in Fig. 4 as motivated from Itskov and Knyazeva (2016) and Verron and Gros (2017) are compared to the Dirac distribution with $N = \mathscr{N} = 7.84$ and $\mu = nkT$, and fracture toughness G_c given by (19). For each type of chain length distribution, where the value of parameter $\mathscr{N}$ is invariant, it is possible to obtain several sets of distribution parameters such that they satisfy the relation between $\mathscr{N}$ and $P(N)$. It is shown that both the effective shear modulus and fracture toughness of the polydisperse elastomer networks can vary significantly from its monodisperse counterparts, depending on the distribution.

3. Phase-field model for polydisperse elastomer networks

In the variational approach to brittle fracture proposed by Francfort and Marigo (1998), the crack initiation and quasi-static evolution are the natural results of the minimization of a Griffith-like energy functional defined as the sum of the elastic energy and the surface energy of the cracked body. The minimization has to be taken among all the kinematically admissible displacements and admissible crack sets, and subject to Dirichlet boundary conditions and an irreversibility condition to avoid unphysical healing of cracks. The quasi-static evolution of brittle fracture under the time-dependent loading parametrized by a pseudo-time, is recast as three principles of irreversibility, global stability and energy balance (Bourdin et al., 2000; Marigo et al., 2016).

The direct numerical implementation of Griffith's energy functional is challenging due to the jump discontinuities of displacements whose locations are a priori unknown. To overcome this challenge, Bourdin et al. (2000) resorted to a regularization strategy initially developed by Ambrosio and Tortorelli (1990) for solving similar free-discontinuity problems encountered in image segmentation (Mumford and Shah, 1989). In the regularized model, cracks are represented by a scalar phase-field, which is 1 inside a cracked zone, 0 away from the crack, and varies from 0 to 1 smoothly. The energy functional of a possibly fractured elastic body with isotropic surface energy is modeled by

$$\mathscr{E}_\ell(\boldsymbol{u}, \lambda_b, \alpha) = \int_\Omega a(\alpha)W(\boldsymbol{u}, \lambda_b)\, d\Omega + \frac{G_c}{c_w}\int_\Omega \left(\frac{w(\alpha)}{\ell} + \ell\|\nabla\alpha\|^2\right) d\Omega, \tag{21}$$

where $a(\alpha)$ is a (decreasing) stiffness modulation function and $w(\alpha)$ is an (increasing) function representing the specific energy dissipation per unit of volume, the $c_w = 4\int_0^1 \sqrt{w(\alpha)}\, d\alpha$ is normalization constant. In the following we will assume

$$a(\alpha) = (1-\alpha)^2, \quad w(\alpha) = \alpha, \tag{22}$$

although different choices are possible, see e.g. Pham et al. (2011) and Marigo et al. (2016). This family of functionals is parametrized by a regularization parameter $\ell > 0$ with units of length dictating the width of the smeared crack that is physically interpretated as an internal length. When ℓ goes to zero, the regularized model converges to the sharp variational theory of brittle fracture in the sense of Gamma-convergence (Bourdin et al., 2008). However the numerical simulations require

Table 1
Different chain length distributions and sets of parameters resulting in the identical parameter $\mathscr{N}$.

Distribution	$P(N)$	Parameters	$\sum_{N=N_0}^{\infty} P(N)N$	μ^*/μ	$G_c{}^*/G_c$
Dirac delta	$\delta(N-N^*)$	$N^* = \mathscr{N} = 7.84$	7.84	1.0	1.0
Exponential	$\begin{cases}\frac{1}{\delta}\exp\left(-\frac{N-N_0}{\delta}\right) & N \geq N_0 \\ 0 & N \leq N_0\end{cases}$	$N_0 = 2.0$; $\delta = 5.058$	7.058	0.900	0.900
		$N_0 = 7.4$; $\delta = 0.434$	7.834	0.999	0.999
Uniform	$\begin{cases}\frac{1}{b-a} & a \leq N \leq b \\ 0 & N < a \text{ or } N > b\end{cases}$	$a = 1.0$; $b = 13.531$	7.265	0.927	0.906
		$a = 5.921$; $b = 9.682$	7.802	0.995	0.995
Weibull	$\frac{a}{b}\left(\frac{N}{b}\right)^{(a-1)}\exp\left(-\left(\frac{N}{b}\right)^a\right)$	$a = 1.25$; $b = 6.846$	6.927	0.884	0.868
		$a = 8.713$; $b = 8.25$	7.801	0.995	0.995
Normal	$\frac{1}{\sqrt{2\pi\delta^2}}\exp\left(-\frac{(N-N_0)^2}{2\delta^2}\right)$	$N_0 = 3.09$; $\delta = 6.596$	7.099	0.905	0.887
		$N_0 = 7.8$; $\delta = 1.104$	7.800	0.995	0.995
Log-normal	$\frac{1}{N\sqrt{2\pi\delta^2}}\exp\left(-\frac{(\ln N - \ln N_0)^2}{2\delta^2}\right)$	$N_0 = 3.0$; $\delta = 1.079$	6.238	0.796	0.787
		$N_0 = 7.71$; $\delta = 0.149$	7.796	0.994	0.994

Please cite this article as: B. Li and N. Bouklas, A variational phase-field model for brittle fracture in polydisperse elastomer networks, International Journal of Solids and Structures, https://doi.org/10.1016/j.ijsolstr.2019.08.012

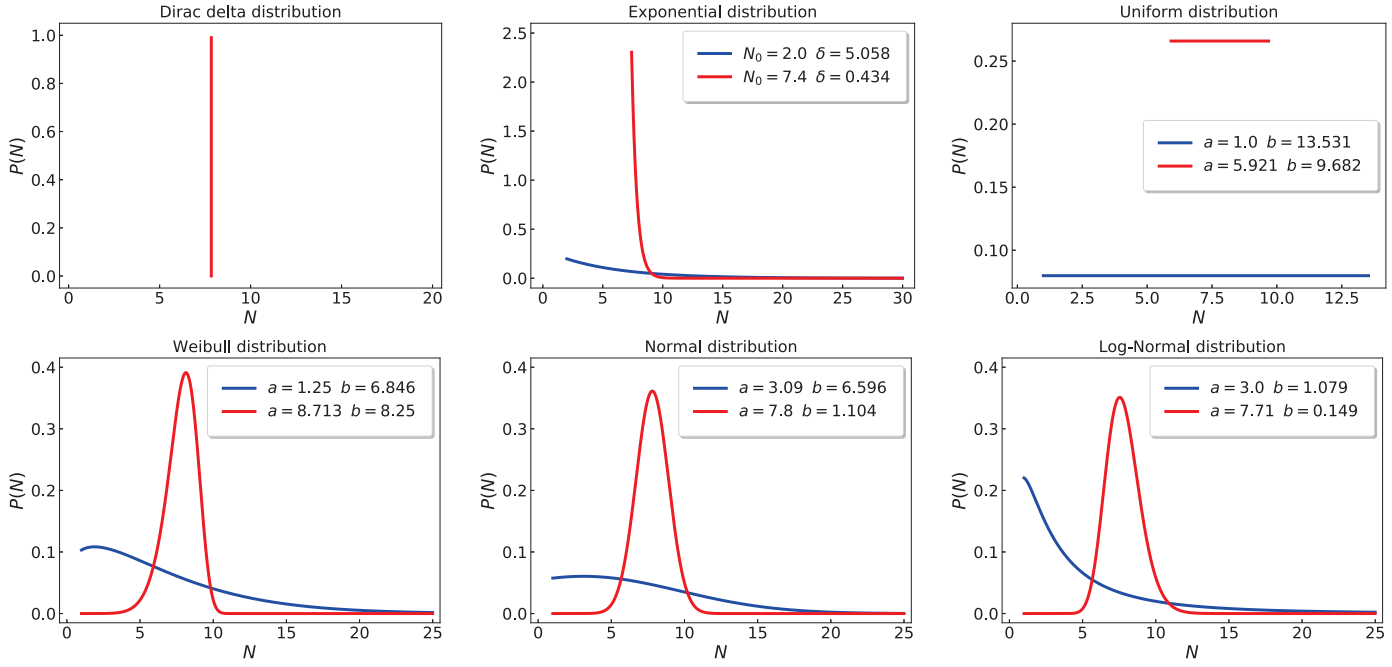

Fig. 4. Different chain length distribution functions corresponding to Table 1.

a finite value of ℓ, which needs to be resolved by the numerical discretization grid, and are based on *local minimization*, instead of global minimality as in Gamma-convergence theory. As discussed in Pham et al. (2011) and Tanné et al. (2018), the phase-field model with a fixed internal length and an evolution principle based on meta-stability (local energy minimization) can be regarded as a gradient damage model, where ℓ become a constitutive parameters related to the maximum allowable stress in the material.

Various numerical simulations have demonstrated that phase-field models can reproduce the onset of crack propagation at Griffith's threshold (Pham et al., 2017; Tanné et al., 2018) and complex crack patterns in brittle materials with anisotropic surface energy (Li et al., 2015; Li and Maurini, 2019), as well as to predict almost quantitatively crack paths in tearing thin sheets (Li et al., 2018). In a quasi-static setting, the theoretical work of Hakim and Karma (2009) pointed out that the principle of local symmetry and maximum energy release rate criteria are embedded in phase-field fracture models. Moreover, analytical predictions of crack paths based on generalized energy release rate criterion have been validated by experiments and numerical simulations for isotropic materials (Pham et al., 2017) and for brittle materials with anisotropic fracture toughness (Li and Maurini, 2019). The success of gradient damage or phase-field model has prompted a large body of literature in mathematics and computational mechanics including several contributions devoted to the nucleation and propagation of crack in elastomeric materials (Miehe and Schänzel, 2014; Talamini et al., 2018; Mao and Anand, 2018; Kumar et al., 2018).

4. Numerical implementation

The numerical implementation of the gradient damage model restricted to compressible materials (Miehe and Schänzel, 2014; Talamini et al., 2018) does not present any specific difficulties. The techniques developed for the linear elastic case, which are not detailed here, are immediately applicable. In the nearly or slightly incompressible setting when the bulk modulus becomes large in comparison to shear modulus, displacement based finite element discretization suffers from the locking phenomenon (Wriggers, 2008; Auricchio et al., 2013). In order to tackle this challenge, Kumar et al. (2018) proposed a scheme based on a non-conforming low order Crouzeix-Raviart finite element discretization with a stabilization term which penalizes the jump of the deformation field across element faces. From a computational point of view, the non-conforming finite element discretization leads to significantly fewer degrees of freedom than competing conforming dicretizations. However, the selection of the value for the penalty parameter is not trivial (Kumar et al., 2018). In this paper we model the polydisperse elastomer networks as an incompressible material and use Lagrange multipliers to enforce the incompressibility constraint.

To impose the incompressibility constraint, we consider the following functional

$$\mathscr{E}_\ell(\boldsymbol{u}, \lambda_b, p, \alpha) = \mathscr{E}_\ell(\boldsymbol{u}, \lambda_b, \alpha) + \int_\Omega p(J-1)\, d\Omega, \tag{23}$$

where the Lagrange multiplier p is equivalent to the hydrostatic pressure field and $J = \det \boldsymbol{F}$ is the determinant of the deformation gradient. However, note that the damage materials are no longer incompressible because of the microcrack growth or crack opening, accordingly the incompressibility constraint should be relaxed in the damaged regions in an appropriate way. To this end, we instead consider a damage dependent relaxation of the incompressibility constraint and the following energy functional is introduced

$$\mathscr{E}_\ell(\boldsymbol{u}, \lambda_b, \alpha) = \mathscr{E}_\ell(\boldsymbol{u}, \lambda_b, \alpha) + \frac{1}{2}\int_\Omega a^3(\alpha) K (J-1)^2\, d\Omega, \tag{24}$$

where we choose to damage the bulk modulus K faster than the shear modulus μ ensuring that the incompressibility constraint does not impose a barrier to the physical opening of crack. Effectively, it allows the damaged phase to bypass the incompressibility constraint. In the intact material incompressibility is ensured by setting the bulk modulus $K \gg \mu$ sufficiently large. However, when applied to the finite element discretization, this formulation near the incompressible limit exhibits severe volumetric locking issue (Wriggers, 2008; Auricchio et al., 2013). To circumvent this numerical difficulties, we resort to the classical mixed formulation and introduce the pressure-like field $p = -\sqrt{a^3(\alpha)K}(J-1)$ as an independent variable along with the displacement field. The constraint

Please cite this article as: B. Li and N. Bouklas, A variational phase-field model for brittle fracture in polydisperse elastomer networks, International Journal of Solids and Structures, https://doi.org/10.1016/j.ijsolstr.2019.08.012

for $p+\sqrt{a^3(\alpha)}K(J-1)=0$ is imposed through a Lagrange multiplier Λ, thus the energy functional is written as

$$\mathscr{E}_\ell(\boldsymbol{u},\lambda_b,p,\Lambda,\alpha)=\mathscr{E}_\ell(\boldsymbol{u},\lambda_b,\alpha)+\int_\Omega\frac{p^2}{2K}\,d\Omega + \int_\Omega\Lambda\left(p+\sqrt{a^3(\alpha)}K(J-1)\right)d\Omega. \tag{25}$$

The stationary point of the energy functional (25) with respect to Λ immediately identifies that $\Lambda=-p/K$, then we arrive at the final form

$$\mathscr{E}_\ell(\boldsymbol{u},\lambda_b,p,\alpha)=\mathscr{E}_\ell(\boldsymbol{u},\lambda_b,\alpha)-\int_\Omega\sqrt{a^3(\alpha)}\,p\,(J-1)\,d\Omega-\int_\Omega\frac{p^2}{2K}\,d\Omega, \tag{26}$$

which is a $\boldsymbol{u}-p$ mixed formulation very much similar with the perturbed Lagrangian multiplier method (Wriggers, 2008), where the last term serves the purpose of regularization of the Lagrange multiplier. We could expect that as the value of $K\to\infty$ the solution obtained from the functional (26) will converge in the sense of weak convergence to the solution given by the classic Lagrange multiplier formulation (23). It is worth noting that a similar formula had been directly introduced in a recent work of Ma et al. (2016). The displacement field $\boldsymbol{u}$ is discretized using standard Lagrange elements of order 2, whilst the pressure-like field p and damage fields α are discretized by linear Lagrange elements. The resulting finite element space for elastic problem falls in the family of the Taylor-Hood elements (Taylor and Hood, 1973) frequently used in solving problems for incompressible flow (Taylor and Hood, 1973), incompressible elasticity and poroelasticity (Bouklas et al., 2015; Cajuhi et al., 2018). This mixed formulation with the specific discretization spaces assures the stability of the discretization scheme and prevents the volumetric locking for large values of the bulk modulus or perturbation parameter K, by satisfying the *inf-sup* condition (Boffi et al., 2013).

We follow the classical alternate minimization algorithm developed by Bourdin (2007) to solve the whole nonlinear problem. In the time-discrete evolution, given the finite element approximation of displacement and pressure fields $(\boldsymbol{u}_h^{(i-1)}, p_h^{(i-1)})$ and damage field $\alpha_h^{(i-1)}$ at the time-step t_{i-1}, the solution at the time-step t_i is found by solving the stationery conditions for the functional (26) under the unilateral constraint $\alpha\geq\alpha_h^{(i-1)}$. The whole nonlinear problem is split into a "deformation" sub-problem, consisting in the solution for $(\boldsymbol{u}, p)$ freezing the damage fields, and a "damage" sub-problem, consisting in the solution for the damage field α freezing the "deformation" fields $(\boldsymbol{u}, p)$. The two sub-problems are solved iteratively at each time-step, until a convergence criterion is satisfied.

In the solution of deformation sub-problem the Kuhn segment stretch λ_b has to be calculated first on each Gauss point, namely, solving the nonlinear algebraic equation (17), which is computation intensive (Talamini et al., 2018). Here we provide an approximate solution for λ_b speeding up the computations. Note that the $\lambda_b>1$ occurs at large chain stretch, as shown in Fig. 1(right), therefore we approximate the inverse Langevin function in (17) as $\mathscr{L}^{-1}(x)\approx 1/(\operatorname{sign}x-x)$ if $0.84136\leq|x|<1$ provided by Bergström (1999). In consequence, (17) can be rewritten as

$$A\lambda_b^3+B\lambda_b^2+C\lambda_b+D=0, \tag{27}$$

where $A=E\sqrt{\mathscr{N}}$, $B=-E\left(\sqrt{\mathscr{N}}+\bar{\lambda}_c\right)$, $C=E\bar{\lambda}_c$ and $D=-\mu\bar{\lambda}_c$. This cubic equation could be further reduced to the standard form Zwillinger (2003), that has three real roots expressed in terms of trigonometric functions providing that $3AC-B^2<0$ which is fulfilled for the current physical problem. Thus, the Kuhn segment stretch λ_b is approximated as (Zwillinger, 2003)

$$\lambda_b=2\sqrt{-\frac{r}{3}}\cos\left(\frac{1}{3}\arccos\left(\frac{3s}{2r}\sqrt{-\frac{3}{r}}\right)\right)+\frac{B}{3A}, \tag{28}$$

with

$$r=\frac{3AC-B^2}{3A^2},\quad s=\frac{2B^3-9ABC+27A^2D}{27A^3}. \tag{29}$$

Although the approximate expression of inverse Langevin function is only valid provided that $\bar{\lambda}_c\lambda_b^{-1}/\sqrt{\mathscr{N}}\geq 0.84136$, it is interesting to see that the approximate solution of λ_b is indistinguishable from the exact solution in the whole chain stretch range, see Fig. 5 (with $E/\mu=1200$) for the comparison of approximated solution and solution using exact inverse Langevin function. The inverse Langevin function in functional (26) is approximated by the best reported Padé approximant given by Jedynak (2017). Inserting (28) into (26), we solve the deformation sub-problem with respect to $(\boldsymbol{u}, p)$ by a Newton based nonlinear solver using a trust region `SNESNEWTONTR` combined with line search integrated in the PETSc library (Balay et al., 2016). In the damage sub-problem, even though the functional is quadratic in α, includes a unilateral constraint due to the irreversibility condition $\alpha\geq\alpha_h^{(i-1)}$. The associated variational inequality, demanding a dedicated nonlinear solver, is solved using the variational inequality solver distributed in the PETSc/Tao library (Dener et al., 2018).

The classical approach to solving the deformation sub-problem involves computing the first Gâteaux derivative of the energy functional with respect to $(\boldsymbol{u}, p)$, which in turn need to be solved using Newton's method by taking a second Gâteaux derivative to yield the tangent "stiffness" matrix (Talamini et al., 2018; Mao and Anand, 2018). Here, the computation of the first and second variational derivative is a complicated task due to the highly nonlinear expression of the Kuhn segment stretch (28) and approximation of the inverse Langevin function (Jedynak, 2017). To this end, we leverage the automatic functional differentiation tool offered by the Unified Form Language (UFL) (Alnæs et al., 2014) integrated in the finite element library `FEniCS` (Alnæs et al., 2015), allowing for a straightforward formulation of the complex custom nonlinear hyperelstic model. Another advantage of this implementation is that the syntax closely mirrors the mathematical abstractions of the variational formulation. Our numerical implementation of the proposed phase-field model is based on the `FEniCS` finite element platform (Alnæs et al., 2015) that allows us to have a concise and efficient parallel open-source implementation of the finite element

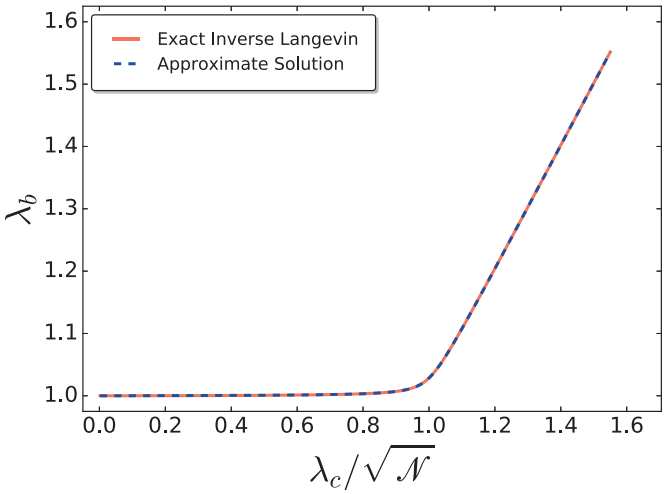

Fig. 5. Comparison of approximated solution and solution with exact inverse Langevin function.

Please cite this article as: B. Li and N. Bouklas, A variational phase-field model for brittle fracture in polydisperse elastomer networks, International Journal of Solids and Structures, https://doi.org/10.1016/j.ijsolstr.2019.08.012

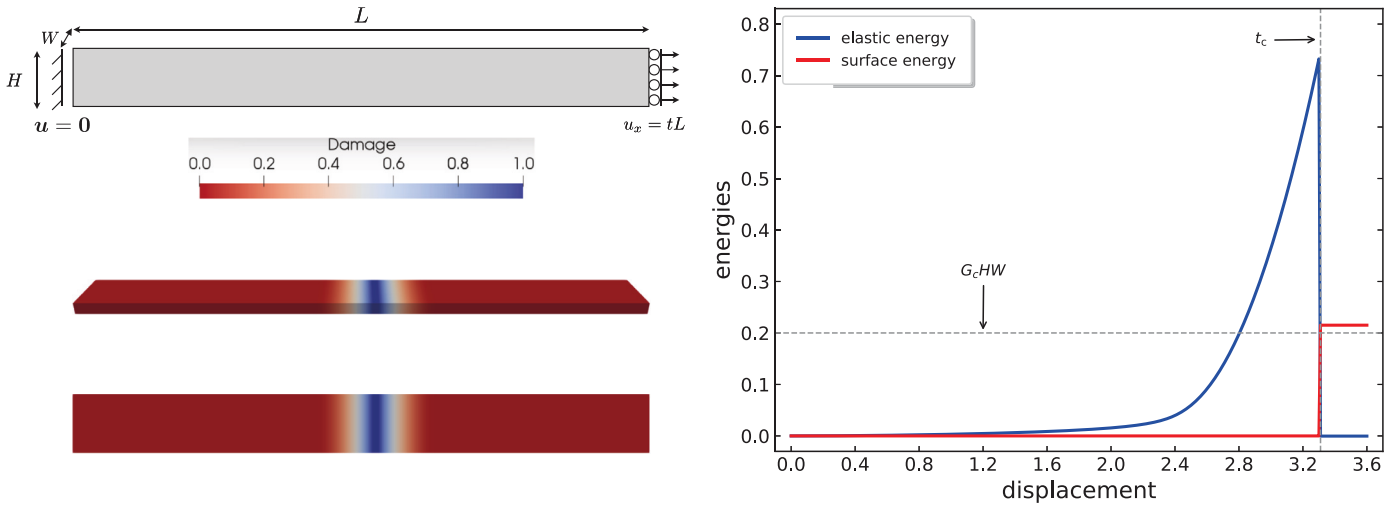

Fig. 6. Three-dimensional uniaxial traction of a hyperelastic bar. (left-top) The imposed boundary conditions: $\boldsymbol{u} = \boldsymbol{0}$ at left end and $u_x = tL$ at right end. (left-bottom) The snapshot of the damage field for $t > t^c$. (right) the evolution of the energies as the end-displacement loading is increased.

model in a few hundreds lines of `python` code distributed as supplementary material of the present paper.[2]

5. Numerical experiments

5.1. Uniaxial tension of a hyperelastic bar

We consider a three-dimensional hyperelastic bar of length $L = 1.0\,\mu\text{m}$, hight $H = 0.1\,\mu\text{m}$ and thickness $W = 0.02\,\mu\text{m}$ in a state of uniaxial stress $\sigma_1 = \sigma$, $\sigma_2 = \sigma_3 = 0$ with the imposed displacement boundary conditions $u_x = 0$ on the left end and $u_x = tL$ on the right end, as illustrated in the Fig. 6(left-top). We also impose the Dirichlet boundary conditions $\alpha = 0$ on the both ends of the bar as in Pham et al. (2011) to force the damage localization to appear inside the bar. Let the stretch along the axis of the loading direction be $\lambda_1 = \lambda$. The incompressibility results in that the stretches in the directions transverse to the axial loading direction are $\lambda_2 = \lambda_3 = 1/\sqrt{\lambda}$. The analytical study of uniaxial tension of a one-dimensional bar developed in Pham et al. (2011) showed that if the length L of the bar is sufficiently larger than the internal length ℓ, the local minimizer of (21) is corresponding to the purely elastic or damage free solution $\alpha = 0$ provided that $t < t_c$. The critical value of t_c is determined by

$$t_c = \frac{2E(\lambda_b - 1)\lambda_b^2\sqrt{\mathscr{N}}}{\mu + E(\lambda_b - 1)\lambda_b} \cos\left(\frac{1}{3}\arccos\left(-\left(\frac{\mu + E(\lambda_b - 1)\lambda_b}{E(\lambda_b - 1)\lambda_b^2\sqrt{\mathscr{N}}}\right)^3\right)\right) - 1, \tag{30}$$

where the λ_b is the solution of the following nonlinear equation

$$a'(0)\left(\mathscr{C}\mathscr{N}\left(\frac{1}{2}E(\lambda_b - 1)^2\right) - \mathscr{C}\mathscr{N}\mu \ln\left(\frac{\mu}{\mu + E(\lambda_b - 1)\lambda_b}\right)\right) + \frac{G_c}{c_w}\frac{w'(0)}{\ell} = 0. \tag{31}$$

To arrive to (31), (17) and an approximation of inverse Langevin function (Bergström, 1999) are used. For the numerical simulation, we consider that the chain legnth follows the Dirac delta distribution $P(N) = \delta(N - \mathscr{N})$ with $\mathscr{N} = 4$. Other materials parameters are $E = 2.5 \times 10^3\,\text{MPa}$, $\mu = 1.25\,\text{MPa}$, $G_c = 10^2\,\text{MJ/m}^2$. The perturbation parameter is set to $K = 1.25 \times 10^6\,\text{MPa}$ and mesh size $h = \ell/5 = 10^{-2}\,\mu\text{m}$ such that the critical end-displacement is calculated as $t_c = 3.311$. Fig. 6(left-bottom) shows the snapshot of a transverse crack nucleated at an arbitrary location cutting the bar into two parts, and the size of the localized damage zone could be analytically evaluated as 4ℓ (Pham et al., 2011; Marigo et al., 2016). The evolution of the energies as the end-displacements increased is depicted in Fig. 6(right), which clearly demonstrates that the critical end-displacement loading t_c and fracture surface energy G_cHW match closely with the theoretical results. We also report the evolution of the volume ratio as the end-displacement loading is ramped up in Fig. 7 to keep track of our enforcement of the incompressibility condition on undamaged material. Fig. 7 shows that prior to crack nucleation and rupture of the bar into two sections the material is indeed incompressible, but once a crack is formed the damaged phase can volumetrically expand.

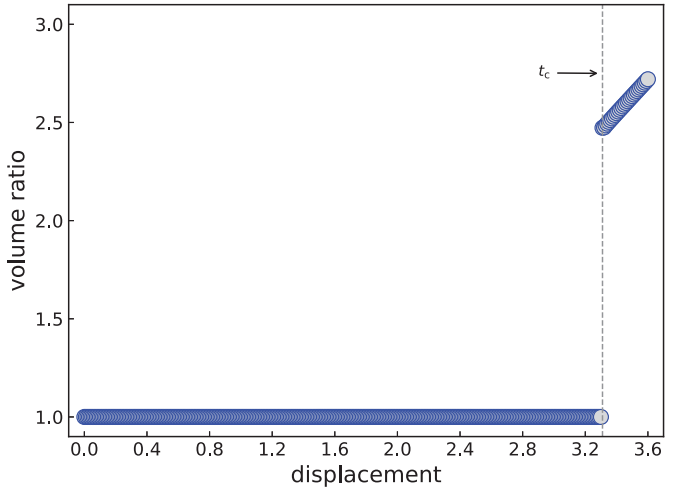

Fig. 7. The evolution of the volume ratio as the end-displacement loading is increased.

5.2. Pure-shear tear experiment

To demonstrate the capability of the gradient damage model to simulate the crack propagation in an incompressible polymer network, we apply the model to simulate the center-cracked

[2] https://bitbucket.org/bin-mech/gradient_damage_polymer/.

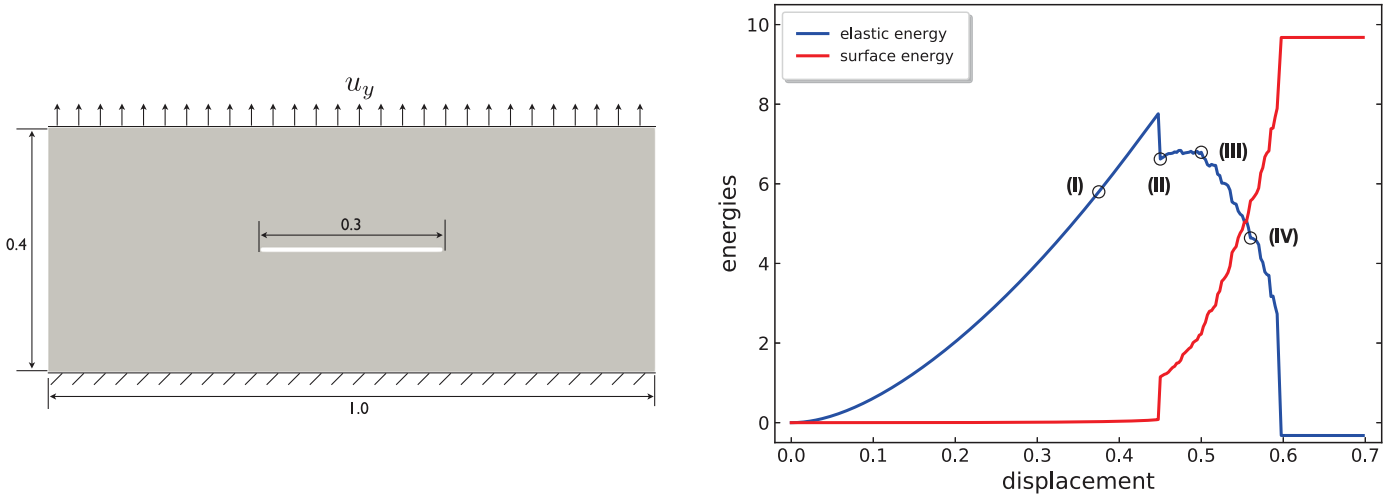

Fig. 8. The specimen geometry (width of 1.0 μm and height of 0.4 μm with a center horizontal notch of 0.3 μm length) and the evolution of the energies of the pure-shear tear experiments.

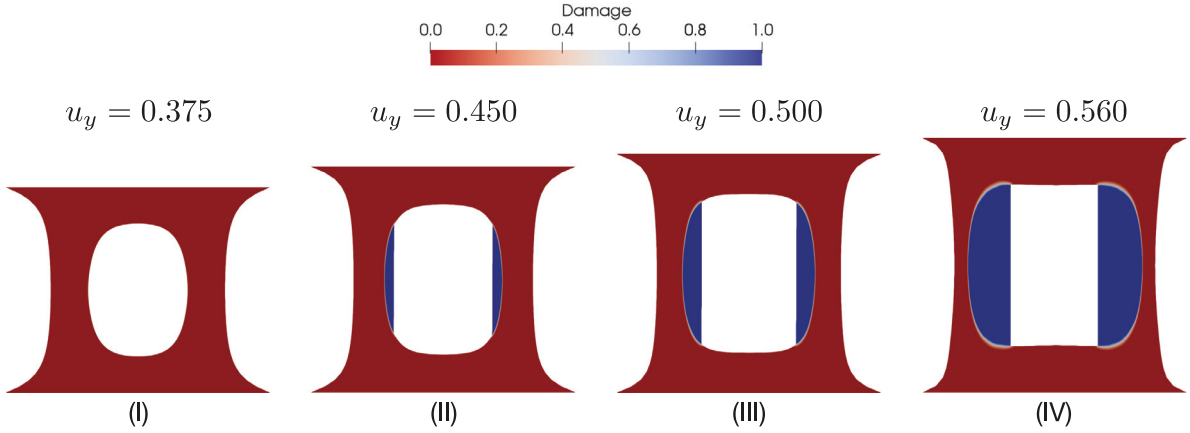

Fig. 9. The snapshots of the pure-shear tear simulation: deformed configuration colored by the damage field.

pure-shear tear experiment. The specimen geometry and applied clamped boundary conditions are schematically depicted in Fig. 8(left). We consider that the chain length follows a geometric distribution (Watson, 1953; Flory, 1953) derived by a statistical treatment of the polymerization process. The probability distribution that a linear polymer molecule is composed of exactly $N \geq N_0$ segments (Watson, 1953; Flory, 1953; Itskov and Knyazeva, 2016) is given by the function $P(N) = q^{N-N_0}(1-q), \quad N = N_0, N_0+1, \ldots,$ where $0 < q < 1$ denotes the probability of addition of a monomer unit to a radical while $1-q$ represents the probability of termination of a radical (Watson, 1953), and N_0 is the arbitrary minimal number of chain segments. It satisfies a priori the normalization condition $\sum_{N=N_0}^{\infty} P(N) = 1$ for any N. Following Itskov and Knyazeva (2016), we express $P(N)$ in terms of the average number of chain segments $\bar{N} = \mathscr{C}\mathscr{N}$, thus $P(N) = 1/(\Delta+1)(1+1/\Delta)^{N_0-N}$, where $\Delta = \bar{N} - N_0$ and $p = \Delta/(\Delta+1)$. The distribution parameters are chosen as $N_0 = 6$ and $\bar{N} = \mathscr{C}\mathscr{N} \approx 11.38$ such that $q \approx 0.84$ and $\mathscr{N} = \left(\sum_{N=N_0}^{\infty} P(N)N\right)^2 / \left(\sum_{N=N_0}^{\infty} P(N)\sqrt{N}\right)^2 = \bar{N}/(1-q)\,\Phi(q, -1/2, N_0) \approx 12$, where $\Phi(z, s, a)$ is a Hurwitz-Lerch transcendent (Gradshteyn and Ryzhik, 2000). The materials parameters are $E = 2.5 \times 10^3$ MPa, $\mu = 1.25$ MPa, $K = 1.25 \times 10^6$ MPa, and the fracture toughness microscopically approximated by (20) is set to $G_c = 12.5\,\mathrm{MJ/m^2}$. In order to resolve the crack properly, the mesh is refined where the crack is expected to propagate such that mesh size $h = \ell/5 = 10^{-2}\,\mu$m.

Fig. 8(right) reports the energy evolution until the ultimate rupture of the specimen, shows the energetic signature of the crack initiation. The snapshot of the deformed configurations of the specimen colored by the damage field are shown in Fig. 9, corresponding to the different loading steps marked in Fig. 8(right), i.e. at prescribed boundary displacements of $u_y = 0.375\,\mu$m, $u_y = 0.450\,\mu$m, $u_y = 0.500\,\mu$m and $u_y = 0.560\,\mu$m. At stage (I), the initial notches are blunted and the cracks have not initiated. The cracks initiate and propagate a finite length associated with a sudden jump of the elastic and surface energy towards stage (II). Further stretching is required to trigger crack propagation until ultimate failure. It is noted that varying the chain length distribution will not affect the crack path evolution, but will influence the loading corresponding to crack initiation and propagation as showcased in Table 1. Contrary to prior studies (Talamini et al., 2018), our model damages energy contributions from both the internal energy and the entropic elasticity. It is also known that at the reference state when $\lambda_c = 1$ entropic elasticity requires that a residual force is acting and thus the energy is not zero at that state. In this plot we take the reference state as a datum, and as the material is fully damaged (over a finite thickness) and elastically unloads following rupture, the entropic energy contribution at the reference state over the damaged material is lost. Thus the total energy at the fully unloaded damaged state falls below the datum. This implication does not have any physical consequence to the model.

Please cite this article as: B. Li and N. Bouklas, A variational phase-field model for brittle fracture in polydisperse elastomer networks, International Journal of Solids and Structures, https://doi.org/10.1016/j.ijsolstr.2019.08.012

Although not shown here, the two cracks emanated from the initial notch tips did not always propagate simultaneously.

6. Conclusions

All synthetic polymers have a distribution of chain length, which occurs naturally during polymerization. The polydispersity has a significant effect on the mechanical behavior of these materials, including the damage and fracture response. A common underlying assumption for the majority of constitutive models for rubber elasticity is that all the chains admit the same length. This is the is the first time the equal force model for polydisperse polymers is extended to include the stretching effect of Kuhn segments and also the first time the equal force model is adapted to the phase-field approach for brittle fracture allowing for the prediction of crack nucleation, initiation and propagation.

In this paper, we formulate a phase-field model for brittle fracture in polydisperse elastomer networks accounting for (1) internal energy contributions from the extension of molecular bonds and (2) arbitrary chain length distributions. An analytical expression for the free energy of the continuum is derived based on the eight chain network model. To be consistent with the Lake-Thomas model for fracture in elastomers, the representative chain in the eight chain network model, consisting of sub-chains with the same distribution of chain lengths, obeys the equal force assumption. We present a mixed displacement-pressure formulation similar to the perturbed Lagrangian multiplier method for the discretization of the incompressible large deformation elastic problem that arises. The numerical simulation agrees very well with the analytical solution for the crack nucleation problem of an incompressible three-dimensional hyperelastic bar under uniaxial loading. On the computational side, we present an approximate analytical expression of Kuhn segment stretch that avoids solving the nonlinear algebraic equation on each Gaussian point during the solution of the large deformation elastic problem contrary to the implementation in Talamini et al. (2018). We employ the FEniCS platform to provide a concise and efficient parallel open-source implementation of the finite element model. We demonstrate the capability of the phase-field model to simulate the crack propagation in an incompressible polymer network through a representative numerical simulation.

A set of interesting future endeavors could include extending the current model to describe both cavitation and fracture (Henao et al., 2016), and considering the non-affine deformation (Diani and Le Tallec, 2019) as well as the effect of entanglements with the neighboring chains (Xiang et al., 2018; Khiêm and Itskov, 2016).

Acknowledgment

Our work was partially supported by the Cornell Center for Materials Research with funding from the NSF MRSEC program (DMR-1719875).

References

Ahagon, A., Gent, A.N., 1975. Threshold fracture energies for elastomers. J. Polymer Sci. Polymer Phys. Ed. 13 (10), 1903–1911.
Alnæs, M., Blechta, J., Hake, J., Johansson, A., Kehlet, B., Logg, A., Richardson, C., Ring, J., Rognes, M.E., Wells, G.N., 2015. The FEniCS project version 1.5. Arch. Numer. Softw. 3 (100), 9–23.
Alnæs, M.S., Logg, A., Ølgaard, K.B., Rognes, M.E., Wells, G.N., 2014. Unified form language: a domain-specific language for weak formulations of partial differential equations. ACM Trans. Math. Softw. (TOMS) 40 (2), 9.
Ambrosio, L., Tortorelli, V.M., 1990. Approximation of functional depending on jumps by elliptic functional via gamma-convergence. Commun. Pure Appl. Math. 43 (8), 999–1036.
Arruda, E.M., Boyce, M.C., 1993. A three-dimensional constitutive model for the large stretch behavior of rubber elastic materials. J. Mech. Phys. Solids 41 (2), 389–412.
Auricchio, F., Da Veiga, L.B.a., Lovadina, C., Reali, A., Taylor, R.L., Wriggers, P., 2013. Approximation of incompressible large deformation elastic problems: some unresolved issues. Comput. Mech. 52 (5), 1153–1167.
Balay, S., Abhyankar, S., Adams, M.F., Brown, J., Brune, P., Buschelman, K., Dalcin, L., Dener, A., Eijkhout, V., Gropp, W.D., Kaushik, D., Knepley, M.G., May, D.A., McInnes, L.C., Mills, R.T., Munson, T., Rupp, K., Sanan, P., Smith, B.F., Zampini, S., Zhang, H., Zhang, H., 2016. PETSc Users Manual. Technical Report ANL-95/11 - Revision 3.7. Argonne National Laboratory. http://www.mcs.anl.gov/petsc.
Bergström, J.S., 1999. Large strain time-dependent behavior of elastomeric materials. Massachusetts Institute of Technology Ph.D. thesis.
Boffi, D., Brezzi, F., Fortin, M., et al., 2013. Mixed Finite Element Methods and Applications, 44. Springer.
Bouklas, N., Landis, C.M., Huang, R., 2015. A nonlinear, transient finite element method for coupled solvent diffusion and large deformation of hydrogels. J. Mech. Phys. Solids 79, 21–43.
Bourdin, B., 2007. Numerical implementation of the variational formulation for quasi-static brittle fracture. Interf. Free Bound. 9 (3), 411–430.
Bourdin, B., Francfort, G., Marigo, J.-J., 2000. Numerical experiments in revisited brittle fracture. J. Mech. Phys. Solids 48 (4), 797–826.
Bourdin, B., Francfort, G., Marigo, J.-J., 2008. The variational approach to fracture. J. Elast. 91 (1), 5–148.
Boyce, M.C., Arruda, E.M., 2000. Constitutive models of rubber elasticity: a review. Rubber Chem. Technol. 73 (3), 504–523.
Cajuhi, T., Sanavia, L., De Lorenzis, L., 2018. Phase-field modeling of fracture in variably saturated porous media. Comput. Mech. 61 (3), 299–318.
Chen, L., Li, B., de Borst, R., 2019. Energy conservation during remeshing in the analysis of dynamic fracture. Int. J. Numer. Methods Eng. doi:10.1002/nme.6142.
Chen, L., Verhoosel, C.V., de Borst, R., 2018. Discrete fracture analysis using locally refined t-splines. Int. J. Numer. Methods Eng. 116 (2), 117–140.
Crist B., Jr, Oddershede, J., Sabin, J.R., Perram, J.W., Ratner, M.A., 1984. Polymer fracture simple model for chain scission. J. Polymer Sci. Polymer Phys. Ed. 22 (5), 881–897.
Dal, H., Kaliske, M., 2009. A micro-continuum-mechanical material model for failure of rubber-like materials: application to ageing-induced fracturing. J. Mech. Phys. Solids 57 (8), 1340–1356.
Dener, A., Denchfield, A., Munson, T., Sarich, J., Wild, S., Benson, S., McInnes, L.C., 2018. TAO 3.10 Users Manual. Technical Report ANL/MCS-TM-322 Revision 3.10. Mathematics and Computer Science Division, Argonne National Laboratory. https://www.mcs.anl.gov/petsc/petsc-current/docs/tao_manual.pdf.
Diani, J., Le Tallec, P., 2019. A fully equilibrated microsphere model with damage for rubberlike materials. J. Mech. Phys. Solids 124, 702–713.
Drury, J.L., Mooney, D.J., 2003. Hydrogels for tissue engineering: scaffold design variables and applications. Biomaterials 24 (24), 4337–4351.
Falender, J.R., Yeh, G., Mark, J.E., 1979. The effect of chain length distribution on elastomeric properties. 1. comparisons between random and highly nonrandom networks. J. Am. Chem. Soc. 101 (24), 7353–7356.
Flory, P.J., 1953. Principles of Polymer Chemistry. Cornell University Press.
Francfort, G.A., Marigo, J.-J., 1998. Revisiting brittle fracture as an energy minimization problem. J. Mech. Phys. Solids 46 (8), 1319–1342.
Gradshteyn, I.S., Ryzhik, I.M., 2000. 8–9 Special Functions. In: Jeffrey, A., Zwillinger, D. (Eds.), Table of Integrals, Series, and Products. Academic Press, San Diego, pp. 851–1038.
Hakim, V., Karma, A., 2009. Laws of crack motion and phase-field models of fracture. J. Mech. Phys. Solids 57 (2), 342–368.
Henao, D., Mora-Corral, C., Xu, X., 2016. A numerical study of void coalescence and fracture in nonlinear elasticity. Comput. Methods Appl. Mech. Eng. 303, 163–184.
Higgs, P.G., Ball, R.C., 1988. Polydisperse polymer networks: elasticity, orientational properties, and small angle neutron scattering. J. Phys. 49 (10), 1785–1811.
Ingraffea, A.R., Saouma, V., 1985. Numerical modeling of discrete crack propagation in reinforced and plain concrete. In: Fracture Mechanics of Concrete: Structural Application and Numerical Calculation. Springer, pp. 171–225.
Itskov, M., Knyazeva, A., 2016. A rubber elasticity and softening model based on chain length statistics. Int. J. Solids Struct. 80, 512–519.
James, H.M., Guth, E., 1943. Theory of the elastic properties of rubber. J. Chem. Phys. 11 (10), 455–481.
Jedynak, R., 2017. New facts concerning the approximation of the inverse Langevin function. J. Non Newton. Fluid Mech. 249, 8–25.
Khiêm, V.N., Itskov, M., 2016. Analytical network-averaging of the tube model:: rubber elasticity. J. Mech. Phys. Solids 95, 254–269.
Kumar, A., Francfort, G.A., Lopez-Pamies, O., 2018. Fracture and healing of elastomers: a phase-transition theory and numerical implementation. J. Mech. Phys. Solids 112, 523–551.
Lake, G.J., Thomas, A.G., 1967. The strength of highly elastic materials. Proc. R. Soc. Lond. A 300 (1460), 108–119.
Li, B., Maurini, C., 2019. Crack kinking in a variational phase-field model of brittle fracture with strongly anisotropic surface energy. J. Mech. Phys. Solids 125, 502–522.
Li, B., Millán, D., Torres-Sánchez, A., Roman, B., Arroyo, M., 2018. A variational model of fracture for tearing brittle thin sheets. J. Mech. Phys. Solids 119, 334–348.
Li, B., Peco, C., Millán, D., Arias, I., Arroyo, M., 2015. Phase-field modeling and simulation of fracture in brittle materials with strongly anisotropic surface energy. Int. J. Numer. Methods Eng. 102 (3–4), 711–727.
von Lockette, P.R., Arruda, E.M., Wang, Y., 2002. Mesoscale modeling of bimodal elastomer networks: constitutive and optical theories and results. Macromolecules 35 (18), 7100–7109.

Please cite this article as: B. Li and N. Bouklas, A variational phase-field model for brittle fracture in polydisperse elastomer networks, International Journal of Solids and Structures, https://doi.org/10.1016/j.ijsolstr.2019.08.012

Lynch, B., Crawford, K., Baruti, O., Abdulahad, A., Webster, M., Puetzer, J., Ryu, C., Bonassar, L.J., Mendenhall, J., 2017. The effect of hypoxia on thermosensitive poly (n-vinylcaprolactam) hydrogels with tunable mechanical integrity for cartilage tissue engineering. J. Biomed. Mater. Res. Part B Appl. Biomater. 105 (7), 1863–1873.
Ma, Z., Feng, X., Hong, W., 2016. Fracture of soft elastic foam. J. Appl. Mechan. 83 (3), 031007.
Mao, Y., Anand, L., 2018. A theory for fracture of polymeric gels. J. Mech. Phys. Solids 115, 30–53.
Mao, Y., Talamini, B., Anand, L., 2017. Rupture of polymers by chain scission. Extreme Mech. Lett. 13, 17–24.
Marigo, J.-J., Maurini, C., Pham, K., 2016. An overview of the modelling of fracture by gradient damage models. Meccanica 51 (12), 3107–3128.
Mark, J.E., 2003. Elastomers with multimodal distributions of network chain lengths. Macromol. Symp. 191 (1), 121–130.
Miehe, C., Schänzel, L.-M., 2014. Phase field modeling of fracture in rubbery polymers. part i: finite elasticity coupled with brittle failure. J. Mech. Phys. Solids 65, 93–113.
Moës, N., Dolbow, J., Belytschko, T., 1999. A finite element method for crack growth without remeshing. Int. J. Numer. Methods Eng. 46 (1), 131–150.
Mueller, H.K., Knauss, W.G., 1971. The fracture energy and some mechanical properties of a polyurethane elastomer. Trans. Soc. Rheol. 15 (2), 217–233.
Mumford, D., Shah, J., 1989. Optimal approximations by piecewise smooth functions and associated variational problems. Commun. Pure Appl. Math. 42 (5), 577–685.
Nonoyama, T., Wada, S., Kiyama, R., Kitamura, N., Mredha, M.T.I., Zhang, X., Kurokawa, T., Nakajima, T., Takagi, Y., Yasuda, K., et al., 2016. Double-network hydrogels strongly bondable to bones by spontaneous osteogenesis penetration. Adv. Mater. 28 (31), 6740–6745.
Pham, K., Amor, H., Marigo, J.-J., Maurini, C., 2011. Gradient damage models and their use to approximate brittle fracture. Int. J. Damage Mech. 20 (4), 618–652.
Pham, K.H., Ravi-Chandar, K., Landis, C.M., 2017. Experimental validation of a phase–field model for fracture. Int. J. Fract. 205 (1), 83–101.
Rivlin, R.S., Thomas, A.G., 1953. Rupture of rubber. i. characteristic energy for tearing. J. Poly. Sci. 10 (3), 291–318.
Smith, S.B., Cui, Y., Bustamante, C., 1996. Overstretching b-DNA: the elastic response of individual double-stranded and single-stranded dna molecules. Science 271 (5250), 795–799.
Talamini, B., Mao, Y., Anand, L., 2018. Progressive damage and rupture in polymers. J. Mech. Phys. Solids 111, 434–457.
Tanné, E., Li, T., Bourdin, B., Marigo, J.-J., Maurini, C., 2018. Crack nucleation in variational phase-field models of brittle fracture. J. Mech. Phys. Solids 110, 80–99.
Taylor, C., Hood, P., 1973. A numerical solution of the Navier-Stokes equations using the finite element technique. Comput. Fluids 1 (1), 73–100.
Tehrani, M., Sarvestani, A., 2017. Effect of chain length distribution on mechanical behavior of polymeric networks. Eur. Poly. J. 87, 136–146.
Treloar, L., Riding, G., 1979. A non-gaussian theory for rubber in biaxial strain. i. mechanical properties. Proc. R. Soc. Lond. A 369 (1737), 261–280.
Treloar, L.R.G., 1975. The Physics of Rubber Elasticity. Oxford University Press, USA.
Verron, E., Gros, A., 2017. An equal force theory for network models of soft materials with arbitrary molecular weight distribution. J. Mech. Phys. Solids 106, 176–190.
Wang, Q., Gossweiler, G.R., Craig, S.L., Zhao, X., 2015. Mechanics of mechanochemically responsive elastomers. J. Mech. Phys. Solids 82, 320–344.
Watson, W.F., 1953. Chain-length distribution functions of polymers after random degradation and cross-linking, with particular reference to elastomers. Trans. Faraday Soc. 49, 1369–1373.
Wriggers, P., 2008. Nonlinear Finite Element Methods. Springer Science & Business Media.
Wu, P.D., Van Der Giessen, E., 1993. On improved network models for rubber elasticity and their applications to orientation hardening in glassy polymers. J. Mech. Phys. Sol. 41 (3), 427–456.
Xiang, Y., Zhong, D., Wang, P., Mao, G., Yu, H., Qu, S., 2018. A general constitutive model of soft elastomers. J. Mech. Phys. Sol. 117, 110–122.
Zhao, X., 2012. A theory for large deformation and damage of interpenetrating polymer networks. J. Mech. Phys. Sol. 60 (2), 319–332.
Zwillinger, D., 2003. CRC Standard Mathematical Tables and Formulae. Chapman and Hall/CRC.

Please cite this article as: B. Li and N. Bouklas, A variational phase-field model for brittle fracture in polydisperse elastomer networks, International Journal of Solids and Structures, https://doi.org/10.1016/j.ijsolstr.2019.08.012